

Inference of Stochastic Dynamical Systems from Cross-Sectional Population Data*

Anastasios Tsourtis[§], Yannis Pantazis[¶], and Ioannis Tsamardinos^{§¶}

Abstract. Inferring the driving equations of a dynamical system from population or time-course data is important in several scientific fields such as biochemistry, epidemiology, financial mathematics and many others. Despite the existence of algorithms that learn the dynamics from trajectorial measurements there are few attempts to infer the dynamical system straight from population data. In this work, we deduce and then computationally estimate the Fokker-Planck equation which describes the evolution of the population's probability density, based on stochastic differential equations. Then, following the USDL approach [22], we project the Fokker-Planck equation to a proper set of test functions, transforming it into a linear system of equations. Finally, we apply sparse inference methods to solve the latter system and thus induce the driving forces of the dynamical system. Our approach is illustrated in both synthetic and real data including non-linear, multimodal stochastic differential equations, biochemical reaction networks as well as mass cytometry biological measurements.

Key words. Population dynamics, Cross-sectional data, Fokker-Planck equation, Weak formulation, sparse dynamics learning

AMS subject classifications. 68Q25, 68R10, 68U05

1. Introduction. In many scientific fields ranging from biology [17], single cell RNA sequencing [21],[18], ecology [31] and epidemiology [3], molecular motion in chemistry, traffic flows in transportation, cross-sectional data over time are gathered. Frequently, researchers can only collect and study cross-sectional data because the same subject cannot be measured again at different time points. For instance, biologists study protein signalling using mass cytometry technologies where each single cell is destroyed during measurement. Time-varying phenomena are typically modelled as deterministic or stochastic dynamical systems such as ordinary differential equations (ODEs), partial differential equations (PDEs), stochastic differential equations (SDEs) and variations. The discovery of the governing equations which drive the natural processes is crucial for the in-depth understanding of the complex interaction mechanisms, for forecasting the evolution of the studied phenomena and for making causal predictions on the effects of interventions. Unfortunately, and despite its usefulness, learning the dynamics of individual populations from cross-sectional data remains largely an open and challenging problem.

Discovering the governing equations from trajectorial data where the same subject is repeatedly measured at a series of time instances has been extensively studied during the last

[§]Computer Science Department, University of Crete, Heraklion, Greece (tsourtis@uoc.gr, tsamard.it@gmail.com).

[¶]Institute of Applied and Computational Mathematics, Foundation for Research and Technology - Hellas, Heraklion, Greece (pantazis@iacm.forth.gr).

*Submitted to the editors December 10, 2020.

Funding: The research leading to these results has received funding from the European Research Council under the European Union's Seventh Framework Programme (FP/2007-2013)/ERC Grant Agreement no. 617393; CAUSALPATH – Next Generation Causal Analysis project.

decade. Typically, a dynamics learning algorithm selects from a rich *dictionary* of non-linear functions (otherwise known as atoms or features or driving forces) which are candidates comprising the unknown system of equations. Given that sparsity is ubiquitous in many physical laws, sparse inference algorithms have been very successful in learning the driving dynamics both for ODEs [5, 20, 14, 7, 28] as well as for PDEs [25, 26, 27], and SDEs [4, 16]. Sparsity is critical for learning large systems from limited data and constitutes a form of complexity penalization and regularization [32, 8, 9]. Sparse optimization regression techniques aim to find the minimal subset of the dictionary that describes the data sufficiently well. Other approaches for dynamics learning based on Monte Carlo Bayesian sampling, [11] and [29] also exist. However, those approaches with the exception of the general framework in [22] are not transferable to cross-sectional data due to the absence of trajectories hence their inability to calculate the derivatives. Indeed, mean-field type approximations where the average trajectory is considered are not satisfactory due to the multi-modality in many cross-sectional datasets.

There exist recent works that approach the subject of system identification based on population data. At the equilibrium or steady-state regime the evolving pdf is not changing, thus data come from a single snapshot of the system. Weinreb et al. [34] used spectral graph theory with the Fokker-Planck formalism [15] in order to predict cell state temporal ordering in single-cell data. Their algorithm output is a unique gene regulatory network, based on multiple assumptions and accompanied by a discussion on limits on ab-initio population data dynamics inference from an equilibrium distribution. Hashimoto et al. [13] rigorously discuss recoverability assumptions of SDE inference both on the equilibrium and transient regime. Their approach is by the use of neural networks on cell differentiation cross-sectional data at few time points, under the assumption that there exists a potential related to the deterministic term in the unknown SDE. Again for dynamical cell differentiation inference, Marco et al. [21] use bifurcation analysis (for binary branching of the data) on evolving pdf's in order to determine the coefficients of a pre-determined potential form (and thus the drift term of the SDE's) along with network, provided that data have sufficient time resolution and low dimension. Krishnaswamy et al. [17] carried out cellular network inference from mass cytometry dynamical population data, based on conditional density resampling statistical techniques. During the final preparation of this paper, we came across the most relevant work to ours, which is under the light of operator approximation instead of differential equations inference. Taylor-King et al. [30] use as well, a weak formulation of the spatially evolving multimodal distributions. On the contrary, we extend the weak formulation to the temporal domain and our adopted Fokker-Planck formulation for SDE's is the analog to their Perron-Frobenius operator. Our algorithm infers the dynamics whereas theirs tracks the evolution of dynamically important states (autonomous states i.e. like a Markov chain). From all the aforementioned works on this field, Hashimoto et al. explicitly infer the unknown functional form of the drift term in the non-equilibrium regime. In [13] and Ma et al. [19] a neural network is used to describe the drift term of the FP equation, whereas in [19] a weak formulation is used in order to connect the F.P. equation with the neural network, while the diffusion term is assumed constant.

We propose a novel population dynamics learning (PDL) algorithm that infers the parameters of the equation that describes the evolution of the data over time. Under the assump-

tion that the cross-sectional data have been generated by a system of stochastic differential equations, the evolution of the data probability density function (pdf) is described by the Fokker-Planck (FP) or forward Kolmogorov equation [12]. Inferring the coefficients of the FP equation from population data is essentially an inverse problem that requires solving the forward problem (i.e., compute the solution of the FP equation). However, this is not feasible due to the high-dimensionality of the FP equation which scales proportionally to the number of variables or species in biochemistry. Instead, we follow the Unified Sparse Dynamics Learning (USDL) framework [22] and considerably extend the theory behind the USDL algorithm. The main technical novelty of this work is the *weak space projection* of FP equation both in time and space, resulting in a transformed yet equivalent atemporal system of equations. This weak space is spanned by appropriately chosen spatio-temporal test functions that best capture the dynamical information of the population data. The integrals involved in the weak space projection are high-dimensional, however, we can statistically estimate them using Monte Carlo approximation. Indeed, an important property of the PDL algorithm is the use of sample averages for the computation of the high-dimensional integrals making the proposed algorithm highly efficient. The last step of PDL algorithm is solving the atemporal system of linear equations using sparse inference algorithms such as Orthogonal Matching Pursuit (OMP) [33] or Lasso [32].

We demonstrate the effectiveness of PDL algorithm with two synthetic and one real dataset examples. The first example is a 2D non-linear SDE system with quadruple-well potential where we show that PDL is capable of correctly identifying the underlying driving forces, deterministic and random terms. This example demonstrates that it successfully recovers a multimodal distribution from population data. The second example is a four variable biochemical reaction network that emulates a signaling pathway cascade of proteins. We show that PDL algorithm learns the biochemical reactions from population data generated from a single experiment (data set), correctly. Additionally, we explore the hyper-parameter space demonstrating that there is a relatively large regime for the hyper-parameters where results are stable. The final example is a set of mass cytometry data [17] that contains protein signalling interactions. PDL algorithm was able to forecast the evolution of the protein populations.

The manuscript is organized as follows. First, the SDE model over the dictionary and the deduced Fokker-Planck equation are presented along with assumptions. In [section 3](#) the weak formulation of the FP equation is derived, with key points over the analytic calculations and numerical setup. The resulting system of integral equations is atemporal and linear with respect to the dictionary items. In [subsection 3.2](#) we show how this reformulation of the problem belongs to the sparse signal recovery field, where a wide range of theoretical tools and algorithms can be utilized to solve it and thus perform (dictionary atom) feature selection. At this point we present our PDL algorithm, where we chose OMP to obtain a sparse solution. Finally in [section 4](#), we demonstrate the efficacy of the PDL algorithm on synthetic and real temporal population data, followed by a discussion on advantages and limitations of our primal approach.

2. Preliminaries.

2.1. Population data. The p -th sample of a time-course dataset (i.e., a non-repeated measurement) at time-point $t_k \in \{t_1, \dots, t_K\}$ is denoted as

$$(2.1) \quad \mathbf{x}_{k,p} := \mathbf{x}_{k,p}^0 + \int_{t_1}^{t_k} dX_t, \quad \mathbf{x}_{k,p} \in \mathbb{R}^N$$

where X_t is the underlying N -dimensional stochastic process while $\mathbf{x}_{k,p}^0 \in \mathbb{R}^N$ are the initial i.i.d. data (i.e., $X_{t_1} = \mathbf{x}_{k,p}^0$). The i.i.d. assumption for the initial data renders the fact that each sample at each time point corresponds to a separate object. For each time-point, P samples that constitute a statistical approximation the probability distribution of the process are given. For the sake of simplicity, we do not consider extra measurement noise and the stochasticity of the data stems solely from the intrinsic randomness of the process.

2.2. SDE Modeling. We assume that the stochastic process $X_t \in \mathbb{R}^N$ is described by a system of stochastic differential equations. An SDE constitutes of two parts: the deterministic part or drift and the stochastic part or the diffusion. We further assume that the drift can be written as a linear combination of potentially non-linear functions as well as the diffusion term has uncorrelated components. Under those assumptions, the mathematical formulation of the SDE is given by

$$(2.2) \quad dX_t = A\psi(X_t)dt + \Sigma dB_t$$

where $A \in \mathbb{R}^{N \times Q}$ is the unknown and typically sparse connectivity (or coefficient or parameter) matrix to be estimated while *dictionary* $\psi(\cdot)$ is a (given) Q -dimensional vector-valued vector function $\psi: \mathbb{R}^N \rightarrow \mathbb{R}^Q$ which contains all the pre-determined candidate functions that might drive the dynamics. Candidate functions are usually powers, cross-products, fractions, trigonometric, exponential or logarithmic functions of the state variables leading to non-linear dynamical systems. $B_t \in \mathbb{R}^N$ is an N -dimensional standard Brownian motion while the diffusion matrix $\Sigma = \text{diag}(\sigma_1, \dots, \sigma_N)$ is diagonal. See Appendix A for detailed explanation.

2.3. Fokker-Planck Equation. The Fokker-Planck (FP) equation describes the probability density *evolution* of a stochastic process that follows an SDE. Let $p(\mathbf{x}, t)$ be the probability of observing the value \mathbf{x} at time t defined by

$$(2.3) \quad p(\mathbf{x}, t) = \mathbb{P}(X_t = \mathbf{x} | \mathbf{x}_0 \sim p_0)$$

Then the FP equation for Equation (2.2) is an $(N + 1)$ -dimensional parabolic PDE given by

$$(2.4) \quad \partial_t p(\mathbf{x}, t) = - \sum_{n=1}^N \mathbf{a}_n^T \partial_{x_n} \{ \psi(\mathbf{x}) p(\mathbf{x}, t) \} + \frac{1}{2} \sum_{n=1}^N \sigma_n^2 \frac{\partial^2}{\partial x_n^2} p(\mathbf{x}, t)$$

where $\mathbf{a}_n \in \mathbb{R}^Q$ is the n -th row of the connectivity matrix A . Our goal is to learn the dynamical equations by solving (2.4), or in other words to determine the non-zero elements of matrices A and Σ .

3. Population Dynamics Learning Algorithm.

3.1. Weak formulation of the FP equation. We proceed with the weak space formulation, which constitutes the transformation of the dynamical system inference to an equivalent atemporal one. This is achieved through the utilization of appropriate test-functions and intuitively, the procedure can be understood as a projection operator that multiplies the system's equation by these test-functions and integrate over time and space. Under this setup, we avoid using a numerical differentiation scheme (such as finite differences) for the crucial and sensitive time derivative computation on the left-hand side of Equation (2.4), like [16, 20]. Subsequently we avoid discretization errors due to long (and possibly uneven) data sampling time intervals, dependent on the sampling time resolution. Additionally, the FP Equation (2.4) as a PDE is high-dimensional in principle, ($N + 1$ dimensions in total) so even a small variable size N renders the integrals (when solving Equation (2.4) for $p(\cdot, t)$) computationally intractable in practice for realistic systems. Thus weak formulation makes it computationally tracktable.

The weak equation partially reverses the derivation procedure to return an integral formulation, which is less strict than the PDE. Essentially it is a projection of the system to a weak space spanned by test functions $\phi_m(\mathbf{x}, t) : \mathbb{R}^N \times \mathbb{R}^+ \mapsto \mathbb{R}, m \in \{1, 2, \dots, M\}$, which will be subsequently differentiated [10].

The weak space FP formulation for Equation (2.4) for $\Sigma = \text{diag}(\sigma_1, \dots, \sigma_N)$ is given by:

$$(3.1) \quad \int_0^T \int_{\mathcal{D}} \phi_m(\mathbf{x}, t) \partial_t p(\mathbf{x}, t) d\mathbf{x} dt = - \sum_{n=1}^N \int_0^T \int_{\mathcal{D}} \phi_m(\mathbf{x}, t) \partial_{x_n} \{a_n^T \psi(\mathbf{x}, t) p(\mathbf{x}, t)\} d\mathbf{x} dt \\ + \frac{1}{2} \sum_{n=1}^N \int_0^T \int_{\mathcal{D}} \phi_m(\mathbf{x}, t) \partial_{x_n x_n} \{\sigma_n^2 p(\mathbf{x}, t)\} d\mathbf{x} dt, \quad m = 1, \dots, M$$

on the spatial domain $\mathcal{D} \subset \mathbb{R}^N$ and time domain $T \in \mathbb{R}$ for the m -th test function. Thus we conclude with a set of M integral equations. We choose test functions in a way that their form is able to capture the data heterogeneity, form and time-scales as we discuss later on. As one can see, the integrals are N -dimensional as the variables $\{X^n\}_{n=1}^N$ are coupled in general. In the following, we define these spatio-temporal functions as:

$$(3.2) \quad \phi_m(\mathbf{x}, t) := \bar{\phi}_{m_1}(\mathbf{x}) \tilde{\phi}_{m_2}(t)$$

meaning that space $\bar{\phi}_{m_1}$ and time $\tilde{\phi}_{m_2}$ have different functional forms in general and $m_1 \in \{1, \dots, M_1\}$, $m_2 \in \{1, \dots, M_2\}$, $M_1 M_2 = M$. We proceed with analytic calculations in Appendix D.

At this point, we stress the fact that the weak space formulation **does not affect the constants** a_{nq} that constitute the unknown matrix A of the inference problem Equation (2.2) if one chose to proceed differently, solving the minimization problem directly as in [5]. In addition, the reader should not confuse the constants in (D.5) with the unknowns a_{nq} .

In subsection 3.2 we proceed with a demonstration of how these equations form N systems of linear equations of order M each. This means that we get Q terms (one row) of the unknown matrix $A \in \mathbb{R}^{N \times Q}$ when solving for each dimension n .

3.1.1. Test functions of the Weak formulation. The role of test functions is vital for the inference problem since it is imperative that they accurately capture the information from the

time domain to the weak space spanned by the chosen test functions. Examples of test functions families are Fourier modes, B-splines, Legendre polynomials, Hermitian polynomials etc. They are required to be smooth, bounded, easy to compute and not necessarily orthogonal. The optimal choice and number of test functions depend on the specific problem at hand and there is no family that can perform optimally for every problem.

B-splines of order k are piece-wise polynomial functions of degree $k - 1$. Their derivatives are lower order polynomials which renders them an attractive choice in the differentiation of the weak form in Equation (D.6). In comparison to the Hermite and Legendre polynomials formerly used in ODE's [22], the B-splines don't drive off to increasingly larger absolute values as their order increases, so the computations contain significantly less numerical errors. B-splines were used as spatial test functions ($\bar{\phi}_{m_1}(x)$) whereas for the time domain we used Fourier modes ($\tilde{\phi}_{m_2}(t)$). The latter constitute varying sinusoidal functions that capture spatial data density changes over time. Figure 1 shows the weak space projection of data $x(t) \sim p(x, t)$, first on spatial test functions $\bar{\psi}_{m_i}(t)$ Figure 1(b) and subsequently on temporal test functions $\hat{\psi}_{m_i, m_j}$ Figure 1(c). Thus, population data are projected over all the combinations of the spatial and temporal test functions. The resulting system of linear equations (d) contains the same unknown constants, as discussed in Subsection 3.2.

3.1.2. Integral Computation with sample estimate. In the weak formulation of PDE's every integral is an inner product (here in L^2), as well as in Equation (3.1). In our problem setup, integrals can be seen as expectations $\mathbb{E}_p(\cdot)$ since the factor $p(x, t)$ is present in every one of them. Thus naive Monte Carlo multi-dimensional integration is feasible [1]. Actually, sampling is the only option in high-dimensional integrals. Moreover, it eliminates the need to approximate the probability density $p(x, t)$ by numerical integration. These attractive properties are very important and allow for a fast and easy implementation. Details on the integral estimators are in Appendix E. The variance of the estimator in Equation (E.1) and consequently in (E.2) is $\mathcal{O}(\frac{1}{\sqrt{P}})$. Note that the weak formulation still contains derivative estimation of the test functions in Equation (D.6) though we are absolved of the finite differences derivative estimation error $\mathcal{O}(\delta t_k)$ and variance $\mathcal{O}(p(x, t_{k+1}) - p(x, t_k))$ associated with $\frac{\partial p(x, t)}{\partial t}$. In addition, a typical finite differences approach would dictate a mesh discretization in N dimensions for every t , which is numerically intractable even for small values of N .

3.2. Solving the Linear System. Upon computation of the integrals over time and space, Equation (3.1) (specifically Equation (D.6)) is written as a system of linear equations:

$$(3.3) \quad Z_{m_1, m_2, n} = \sum_{q=1}^Q a_{nq} \tilde{\Psi}_{m_1, m_2, n, q} + \frac{\sigma_n^2}{2} W_{m_1, m_2, n}, \quad n = 1, \dots, N$$

where the unknowns are a vector of coefficients $\mathbf{a}_n \in \mathbb{R}^Q$ plus diffusion coefficient $\sigma_n \in \mathbb{R}$. $Z_{m_1, m_2, n}$ contains the projected time derivatives of the density function $p(X, t)$ on the m_1 -th spatial and m_2 -th temporal test functions. Respectively, $\tilde{\Psi}_{m_1, m_2, n}$ constitutes the data in dictionary space, $W_{m_1, m_2, n}$ the diffusion component, both subsequently projected onto weak space. One can think of $\tilde{\Psi}$ as feature "transformation" of constructed feature matrix Ψ . For

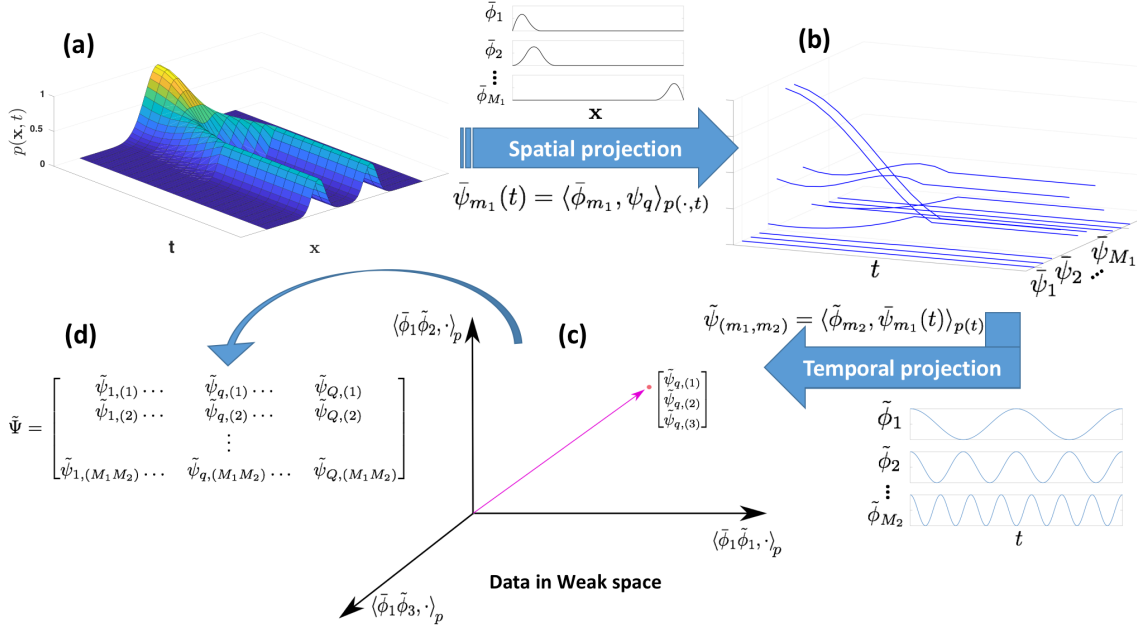


Figure 1. Visual depiction of weak space projection over spatial and temporal test functions. (a) Known one-dimensional evolving bimodal pdf $p(x, t)$ to be learned. We show the continuous-time pdf for better visualization, though PDL algorithm considers time-course measurements at discrete time points. (b) Projection of q -th dictionary atom, based on data from $p(x, t)$, on $M_1 = 11$ spatial B-spline test functions throughout the temporal range $[0, T]$ (continuous-time visualization, q -th atom is chosen linear). The initial distribution $p_0(x)$ gradually splitting, is mostly captured by test-functions $\bar{\phi}_6(x), \bar{\phi}_7(x)$, whereas the two equilibrium modes of x are primarily captured by $\bar{\phi}_4(x), \bar{\phi}_5(x), \bar{\phi}_8(x), \bar{\phi}_9(x)$, because of their support. (c) Second projection of the data, formerly projected in space, over 3 temporal Fourier test functions of varying frequency (M_2 in total). Here only 3 are shown due to the high dimensionality of the $M_1 M_2$ combinations and one (out of Q) dictionary atoms. Eventually we get $M_1 M_2 = M$ such spatio-temporal projections $\langle \bar{\phi}_{m_1} \bar{\phi}_{m_2}, \cdot \rangle$ as shown in Equation (D.1). (d) Resulting matrix of a system of M linear equations in the weak space, for Q dictionary atoms, as described in Equation (3.4) ($n = 1$). Vector Z is obtained by similar projection involving the temporal derivatives $\partial_t \bar{\phi}(t)$.

the n -th variable, the linear system is given by:

$$(3.4) \quad Z_n = \tilde{\Psi}_n \mathbf{a}_n + \frac{\sigma_n^2}{2} W_n = \tilde{\Psi}_n^{\text{aug}} \mathbf{a}_n^{\text{aug}}$$

where $Z_n \in \mathbb{R}^M$, $\tilde{\Psi}_n \in \mathbb{R}^{M \times Q}$, $\mathbf{a}_n \in \mathbb{R}^Q$, $W_n \in \mathbb{R}^M$ and can be solved in the least-squares sense (see next section). **Note** that due to (D.4) there is dependence of $\tilde{\Psi}$ on n . Thus we independently solve N linear systems of the form (3.4).

The usual approach of other works concludes to a linear system of equations such as Equation (3.3), without the integrals, and having a separate system for each time point. In effect, the dimensionality of the problem increases with measurements size whereas in our proposed USDL methodology, time is captured in the atemporal Equation (3.3) of predefined size M , dependent on the input data smoothness. Hence there is no need for smoothing or subsampling (or block averaging) for computational cost reduction and convergence.

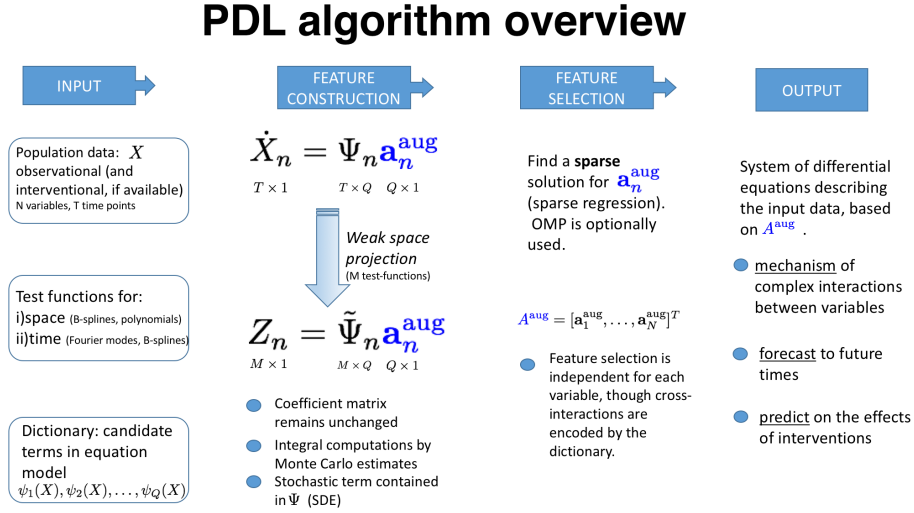


Figure 2. Overview of PDL algorithm for learning SDE's. Note that the weak space projection does not affect the coefficient matrix A , on which a sparse solution is required. The problem is projected to an atemporal equivalent, of dimensionality M .

3.2.1. Minimization problem. Upon computation of matrices Z_n , $\tilde{\Psi}_n$ and W_n , the system (3.4) is written as:

$$(3.5) \quad Z = \Psi a$$

where we have appended the extra unknown σ_n in vector \mathbf{a}_n (also appended vector W_n in array $\tilde{\Psi}_n$) and dropped the index n and \sim for simplicity of notation.

Solving (3.5) for a lies in the category of regression problems. The resulting systems are over-determined because we use a large number of test functions and a broad family of potentially useful dictionary atoms, and a least-squares type minimization of the form $\min \|Z - \Psi a\|$ over a , does not have a sparse solution but a full (dense) one. In practice, a dense solution means that there is a high correlation of the available candidate features (columns of Ψ) as a result of noise in the data (ill-conditioned matrix Ψ) and sparse regression is preferable. To achieve this, a minimization problem with penalization is solved instead:

$$(3.6) \quad \min_a \|a\|_0 \quad \text{subject to} \quad \|Z - \Psi a\|_2 \leq \epsilon,$$

which uses the L^0 norm over the minimization, where $\|a\|_0$ is the number of non-zero elements in a and ϵ is the regression error.

In this work, learning is performed by determining a small subset of important features from an over-determined set of possible features (Q in total), using a non-convex sparse regression greedy algorithm termed Orthogonal matching pursuit (OMP), that approximately solves problem (3.6). Apart from being fast, OMP has the important property that its hyper-parameter is easy to interpret and approximate from the input data. Another convenient attribute of OMP is that of adding prior knowledge, over the set of features describing the

unknown driving forces, in a straightforward way (see [Subsection 4.1](#)). This is important in applications where the user has a partial knowledge on the equation terms or performs interventions in a systematic way (see [Appendix G](#)).

Details on the minimization problem can be found in [Appendix F](#).

3.3. PDL Pseudocode. The PDL algorithm is summarized in [Algorithm 3.1](#) as well as in [Figure 2](#). In case that the input consists of one time-series (trajectory), the former version of USDL [[22](#)] is applicable.

Algorithm 3.1 PDL (Population Dynamics Learning)

Input: population data: P observations of N variables over K time points: $S = \left\{ x_1^p(t), \dots, x_N^p(t) \mid t = t_1, \dots, t_K \right\}_{p=1}^P$, dictionary $\psi_{1:Q}(x)$, set of test functions in time and space $\{\phi_m\}_{m=1}^M$. When data from (R) interventions are present, $S = \{S^1, \dots, S^R\}$
Output: Inferred \hat{A} s.t. $Z = \tilde{\Psi}\hat{A}$

```

1:  $\Psi = \text{comp\_psi}(S)$  ▷ data on dictionary (basis)  $\in \mathbb{R}^{T \times Q \times N}$ 
2: // Compute Weak Space projections  $Z, \tilde{\Psi}, W$ 
3: for  $n = 1, \dots, N$  do
4:   for  $r=1, \dots, R$  do
5:     for  $m=1, \dots, M$  do
6:        $z_{n,m}^{(r)} \leftarrow \mathbb{E}_{p(x_n^{(r)};t)}[\partial_t \phi_m(x_n^{(r)}(t), t)]$  ▷ sample estimate for integral using ((E.2))
7:       for  $q=1, \dots, Q$  do
8:          $\tilde{\Psi}_{n,m}^{q,(r)} \leftarrow \mathbb{E}_{p(x_n^{(r)};t)}[\partial_{x_n} \phi_m(x_n^{(r)}(t), t) \psi_q(\mathbf{x}^{(r)})]$  ▷  $\psi_q$ :  $q$ -th column of  $\Psi(, n)$ 
9:       end for
10:       $w_{n,m}^{(r)} \leftarrow \mathbb{E}_{p(x_n^{(r)};t)}[\partial_{x_n x_n} \phi_m(x_n^{(r)}(t), t)]$ 
11:     end for
12:   end for
13:    $Z_n \leftarrow [z_{n,1:M}^{(1)}, \dots, z_{n,1:M}^{(R)}]$  ▷  $\in MR$ 
14:    $W_n \leftarrow [w_{n,1:M}^{(1)}, \dots, w_{n,1:M}^{(R)}]$ 
15:    $\tilde{\Psi}_n \leftarrow [\tilde{\Psi}_{n,1:M}^{(1)}, \dots, \tilde{\Psi}_{n,1:M}^{(R)}]$  ▷  $\in M \times Q$ 
16:    $\mathbf{a}_n = \text{OMP}(Z_n, \tilde{\Psi}_n, W_n)$  ▷ Solve sparse regression using OMP
17: end for
18: Estimate relative error
19: return  $\hat{A} = [\mathbf{a}_1, \dots, \mathbf{a}_N]^T$  ▷  $\in N \times Q$ 

```

4. Experimental results. In this section we demonstrate the performance of our proposed PDL algorithm ¹ on three different example paradigms; from synthetic multi-dimensional problems with known solutions ([subsections 4.1](#) and [4.2](#)) to a real data problem ([subsection 4.3](#)). We seek a parsimonious dynamical model with as few (non-linear) terms as possible, representing the available data.

¹The code is available online at: [https://github.com/mensxmachina/...](https://github.com/mensxmachina/)

4.1. Learning the dynamics of a multimodal (joint) distribution. Our first system under study is based on multimodal SDE's of two variables of different time scales and intrinsic stochastic noise. The drift term of each variable consists of a double-well potential (non-linear, fourth order) and both terms are of the same functional form with different coefficients resulting to low and high equilibration times of the corresponding stochastic processes x_1, x_2 . We chose this well-studied paradigm because it is used to model a wide range of physical, financial and other phenomena, having the intrinsic difficulty of sample concentration on two modes over time. This data peculiarity, renders existing approaches of: a) averaging-out samples per time point towards a single trajectory or by b) averaging multiple trajectories into fewer in order to reduce computational cost and convergence issues, not applicable. The two-variable system of SDE's is given by:

$$(4.1a) \quad dx_1 = -(x_1^3 - x_1)dt + \sigma_1 dW_1$$

$$(4.1b) \quad dx_2 = -(x_2^3 - 0.5^2 x_2)dt + \sigma_2 dW_2$$

The deterministic drift term $a(x_1, t)$ consists of a double-well potential U whose force is

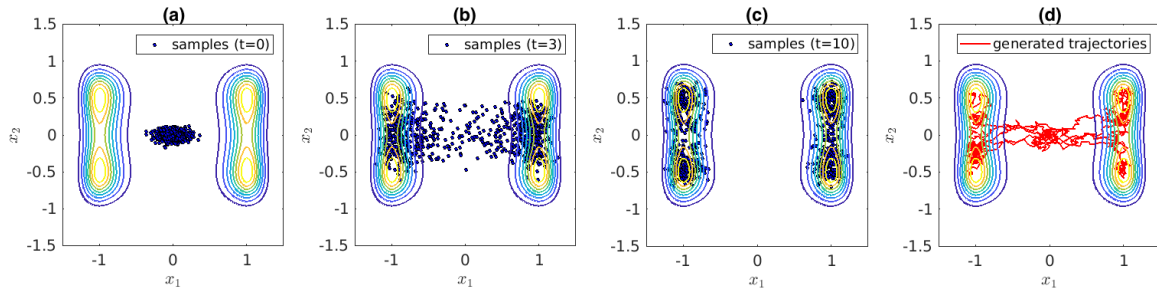


Figure 3. (a) – (c) Time-course (population) data evolution, of bimodal stochastic processes x_1, x_2 of Equation (4.1), measured at (a) initial, (b) transient and (c) steady-state times (blue dots). Contours in each plot correspond to the steady-state pdf. The quadruple-well potential of this system restricts samples in four variable minima centered at: $\{-1, -0.5\}, \{-1, 0.5\}, \{1, -0.5\}, \{1, 0.5\}$, so simple averaging of the data along each variable would result to samples around $\{0, 0\}$ and inference is bound to fail. The noise coefficients are $\{\sigma_1 = 0.2, \sigma_2 = 0.1\}$, resulting to larger variance of samples for process x_1 . (d) Upon inference of the system (4.1) based on time-course data, we generate stochastic trajectories (red solid lines) starting from the initial distribution centered at $\{0, 0\}$. This qualitative visualization shows agreement with input data, as the trajectories converge to the steady-state (or equilibrium) minima. In Figure 4 we show quantitative results.

$a(\mathbf{x}) = -\nabla U(\mathbf{x}) = -\nabla\left(\frac{x_1^4}{4} - \frac{x_1^2}{2}\right) = -(x_1^3 - x_1)$. Figure 3 shows how the joint population data distribution of x_1 and x_2 evolves in time, approaching four potential minima. The importance of this demonstration lies in that our proposed PDL algorithm can handle multimodal population data, meaning that the initial distribution of samples splits into two sample regions as time progresses (see Figure 3). The known nonlinear analytic Equation (4.1) is used to generate noisy data of different stochastic noise level σ_n , given as input to our PDL algorithm.

A polynomial dictionary including at least up to cubic terms is sufficient for this example, though we experimented with higher order dictionaries as well (see supplementary). In principle, richer dictionaries express the dynamics better while on the same time sparsity penalizes possible overfitting, though higher order terms can compensate for lower order ones and in the presence of highly noisy data, falsely provide a different solution due to uniden-

tifiability. For this two-dimensional case, the dictionary consists of 10 variable-combination terms in total; $\psi(x) = \{1, x_1, x_2, x_1x_2, \dots, x_2^3\}$. The inference problem (3.4) lies in defining the multiplicative constants of these terms $\mathbf{a}_n = [a_{n,1}, \dots, a_{n,10}]$, for each variable, plus the diffusion constants σ_1, σ_2 . Hence structure (feature selection of active terms in the dynamics) and parameter estimation (coefficients of active terms) is achieved. The approximated matrix \hat{A} having rows consisting of these multiplicative coefficients for each variable, is termed connectivity (or parameter or coefficient) matrix.

A lower value in the linear term constant in (3.4) (shallower double-well) results to slower convergence of the corresponding process, so for a successful inference across variables, the data should capture the dynamics of all the variables. According to the available data, an appropriate choice on the number of test functions (in space and time) has to be made; less test functions (space: bigger discretization dx intervals, time: low frequency modes) result to a *coarser zoomed-out overview of the dynamical information* whereas utilization of a large number of test functions (very fine dx mesh, additional high frequencies) results to poor sampling of the integrals in the weak formulation, given the fact that the number of time points and samples per time point of the dataset remain fixed.

The test functions used for this example are M_1 quadratic B-splines in space and M_2 Fourier modes in time. We determined that $M_1 = 16$ and $M_2 = 31$ suffice and thorough experimentation for setting hyper-parameters can be found in the supplementary material. The support of the B-splines used here, is defined by the range of each variable and by the variance of each cloud. In other words, the interval length under the non-zero area of a B-spline should be comparable to the average variance of the clouds of samples, in order to **decipher their displacement**. In this example case, the average cloud width of variable x_1 is 0.4 whereas for x_2 is 0.2, meaning that the support of each B-spline should be in this range. By employing $M_1 = 16$ equally spaced B-splines over $[-2 : 2]$, their support is 0.25, resulting to the model with the smallest relative error (discussed in more detail in the next section and in the Supplementary Material).

For this example system, we generate NoS trajectories of Equation (4.1) per intervention, via the Euler-Maruyama numerical integration scheme. A key assumption of population data is that samples are destroyed upon measurement (on measurement time points), so every sample comes from a different realization of dynamics up to that time point. Interventions are randomly picked activations (as discussed in Appendix G) from a pool of initial configuration distributions $\{p_0^1(\mathbf{x}), p_0^2(\mathbf{x}), \dots\}$ (see Supplementary). From a dynamical systems point of view, it is not guaranteed that spawned trajectories from a single small subset p_0 of the spatial domain can explore the system phase space thoroughly. In our case this translates in a roughly evenly spread amount of trajectories between the two meta-stable regions of the double well over time. For this reason, we employ additional activations (additional data sets) in order to correctly identify the terms involved in the underlying equation, that is, to include all the dominant terms (100% recall) and exclude additional terms (100% precision). Figure 4 shows the performance of the PDL algorithm over multiple interventions. As the number of samples increases (red line), the accuracy of the algorithm improves. The same holds when additional interventional data in the form of activations are included. The ‘‘relative error’’ a posteriori metric (defined as $rr = \frac{\|\hat{A} - A\|_2}{\|A\|_2}$) dictates improved inference as well.

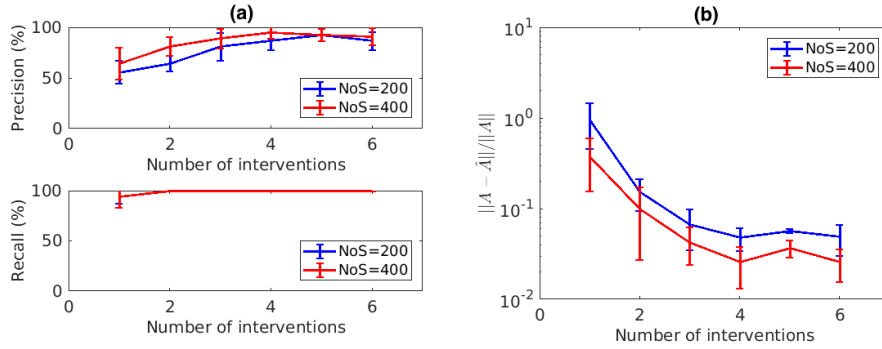


Figure 4. Quantitative estimation of quality of inference for the quadruple-well example. (a) Precision and recall curves for increasing number of interventions having 200 and 400 samples per measurement time point (cloud of samples). Interventions are activations with randomly picked initial distribution p_0 , providing rich dynamical information, improving the identifiability of the unknown system. Matrix A contains the coefficient of each constructed feature which are candidate terms of the unknown system of differential equations (see Figure 2). Precision and recall indicate that the structure of inferred coefficient matrix \hat{A} is recovered as we employ more activations. In addition, the relative error (b) measures the distance of inferred \hat{A} coefficients from the true A . Error bars are calculated over 6 (IID) iterations (each including randomly picked activations from a set of initial distributions $p_0(\mathbf{x})$). $M_1 = 16$ B-splines spatial test functions and $M_2 = 31$ Fourier modes are used (more information on the setting of these parameters can be found in the Supplementary).

4.2. Inducing the dynamics of a synthetic protein reaction network: Cascade. We proceed with another synthetic data example system based on mass-action kinetics and carry out network inference from the recovered differential equations. We construct population data from a four-variable stochastic reaction system (Figure 5(b)) by generating multiple trajectories starting from an initial distribution $p_0 \sim \mathcal{N}(0, \Sigma_0)$. The motivation is the thorough understanding of the PDL inference capabilities and limitations, in a complex system that can be tuned in every aspect. Generalizations of this kind of dynamical systems (reaction networks) are applicable to various scientific/industrial fields and in Subsection 4.3 we proceed with real mass-cytometry data resembling this paradigm. Depending on the choice of dictionary one can, in principle account for unary, binary (i.e. $x_1 \rightarrow x_2 x_3$) or higher order species (variable) interactions, though we restrict to the linear case (Figure 5).

In biochemical kinetics applications, each variable might be a set of protein or gene abundances x_1, x_2, \dots, x_N involved in N reactions. Each reaction n is characterized by a propensity vector containing the reaction rates k_1, \dots, k_Q plus the diffusion coefficient σ_n , which are unknown and constitute the n -th row of matrix A . Our primary goal is to infer the sparse matrix A and in effect, from its structure recover the ground truth reaction network of interacting variables Figure 5(a). Matrix A encodes the direct causal interactions within the set of variables, so if element a_{nq} is zero, then no direct causal interaction from x_n to x_q exists.

Figure 6 shows the population data distribution evolving in time along with generated trajectories upon inference of the dynamical system with the PDL algorithm (red solid lines). Success of inference is not affected for this one-intervention (activation) data example, as long as the time difference between clouds dt in regions of steep dynamics is relatively small. For instance, we set measurement time difference $dt = 0.5$ time units between clouds, because the steepest derivative (fast dynamics) in the interval $[0 : 20]$ is that of variable x_1 . In

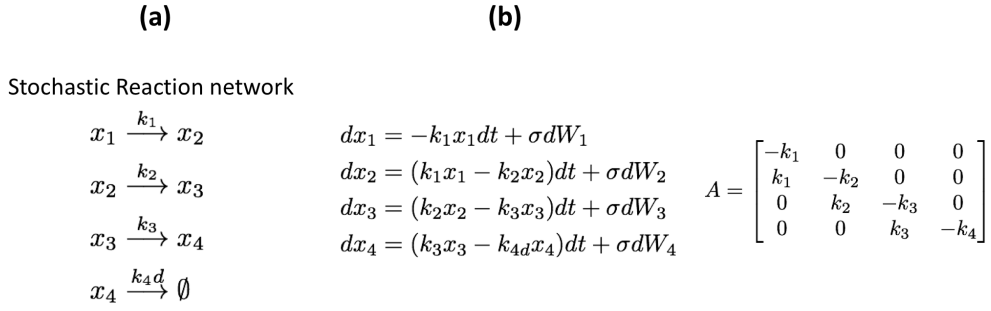


Figure 5. (a) System of four Stochastic Differential equations resembling a reactions network cascade of four proteins (variables). x_1 is converted to x_2 at rate k_1 , x_2 to x_3 at rate k_2 , x_3 to x_4 at rate k_3 and x_4 is depleted at rate k_4d . (b) Linear SDE system which corresponds to (a), compactly written as $\dot{X} = AX + \Sigma W$. The last term in each equation is the diffusion, W_n is a Brownian motion and constant σ diffusion coefficients as in [Subsection 4.1](#). Training data are generated by simulating multiple trajectories of (b), each starting from an initial distribution p_0 . Then samples per measurement time point constitute a cloud and collectively clouds are the population data, given as input to the PDL algorithm. Ultimately we infer the approximated connectivity matrix \hat{A} consisting of the reaction rates k_q and thus, from the structure of \hat{A} , recover the variable network in (a).

real biochemical reaction sampling, measurement time points are very scarce, two orders of magnitude less than the measured samples per time point and pairwise further away as time progresses. The sequential association (pairwise coupling of a cascade) between variables in this specific demonstration implies, that unsuccessful inference of the first variable, affects correct prediction of trajectories of the whole system. The inference breaks down for this example for $dt \geq 0.8$, where the rate of change in abundance of x_1 is very steep to be accurately captured. For this reason, inference is equally satisfactory (wrt relative error) if we set $dt \geq 0.8$ in the interval $[20 : 50]$ and while maintaining $dt = 0.5$ in $[0 : 20]$. In practice, despite the scarcity of measurement times, protein abundances smoothly increase and subsequently decrease as shown variables x_2, x_3, x_4 so variable x_1 is an exaggerated example. On the other hand, the noise σ (associated with the variance of each cloud) should not be very high with respect to the range of the propagating mean protein abundance, as very high signal-to-noise (SNR) ratio can interfere with the recovery of a meaningful solution \hat{A} (by meaningful we imply that generating new data based on inferred \hat{A} , the trajectory neither diverges nor underfits the training data). This is an unidentifiability problem because many SDE systems can be candidate solutions. As demonstrated in the quadruple-well example, additional data from interventions improve the learnt system and can compensate for high SNR. In [Figure 6](#) we have separated the data in training (blue) and test (black) subsets, corresponding to different time intervals. In this way we assess the success of the generated model in forecasting. An extrapolation method would fail to capture the curvature, whereas by learning the governing equations, projection in time is accurate.

4.2.1. Setting algorithm hyper-parameters. Next we quantify the impact of the data parameters of: number of samples NoS , sampling interval dt and algorithm parameters: M_1, M_2 , that need to be tuned for the successful inference of the unknown system. The ground truth A is known, so a metric such as the L_2 distance or “relative error” is used

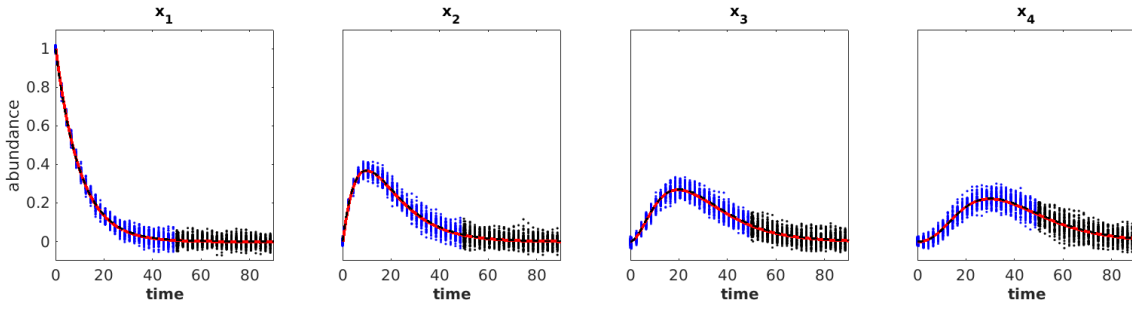


Figure 6. Population data (dots) for the four-variable system of SDE's (synthetic protein Cascade) of Figure 5. The training data up to time $t = 50$ are shown in blue, whereas the test data (black) lie in the time interval $[50 : 90]$. The training data are given as input to the PDL algorithm and inference of the unknown connectivity matrix \hat{A} represents a system of SDE's similar to Figure 5 (b). Next, we simulate the SDE dynamics based on \hat{A} using a numerical scheme, and generate a trajectory, here shown in red solid lines and estimate the goodness of fit in the training set (for clarity, we set the $\sigma = 0$ although it is accurately recovered). In addition, the test set provides a test bed for forecasting of the identified system, where other methods such as extrapolation (eg using Bezier curve) would fail to capture the curvature of the dynamics. Since variables x_1, x_2, x_3, x_4 depend sequentially, each one's intrinsic stochastic noise $\sigma_n dW_n$ propagates along time in the form of increasing variance until reaching a steady state where it remains constant (here $\sigma_n = 0.01$ for all four variables). For comparison, we used SINDy with a linear dictionary and as input, one average time series based on 80% of randomly peaked samples of each cloud. The generated trajectories from \hat{A} by SINDy are shown in black dotted lines and the inferred \hat{A} is almost correct, although SINDy is not designed to recover the stochastic noise coefficient of the SDE's. Both algorithms attain a relative error of 0.02 with respect to the ground truth connectivity matrix A , so the network in Figure 5 is recovered. We conclude that PDL attains good forecasting for various stochastic noise levels, with the added benefit of noise coefficient inference over SINDy.

here. Otherwise we use the L_2 average distance between the generated trajectories based on \hat{A} and input data averages, as a metric (subsection 4.3). Figure 7(a) shows the expected reduction in the relative error with increasing number of samples per cloud NoS , by improving the estimation of the integrals in Equation (3.1) thus reducing statistical noise. Even for $NoS = 100$, the principal terms (the terms present in every \hat{A} estimate over randomly chosen test data sets) in the recovered solution \hat{A} are very close to those of the ground truth A and a plateau is reached over $NoS = 350$. We note that the relative error metric based on the inferred matrix \hat{A} and ground truth A is not an unbiased estimator, meaning that we cannot get arbitrarily close to zero by using more samples.

In Figure 7(b) we see the effect of sparser sampling times (higher dt) on the relative error. As intuitively expected, when the clouds are further away over the same time horizon, the dynamical information is less and the system becomes less identifiable as discussed in the beginning of subsection 4.2. Sparser sampling times when fast dynamics occur, negatively affect the projected derivative estimation on the left hand side of Equation (3.4) and consequently the relative error. For this system we observe a sharp increase in the relative error for $dt \geq 0.8$ time units.

In Figure 7(c), as the number of spatial test functions (B-splines) M_1 increases, the support of each B-spline is narrower since the range of the spatial domain remains fixed at $[-0.2 : 1.2]$ as defined by the training data (abundance range). In effect, the sampling of each integral of the weak form in Equation (D.6) is based on less samples thus providing a worse estimate.

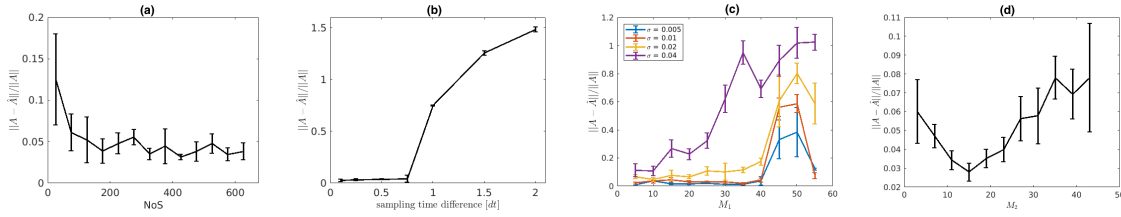


Figure 7. PDL hyper-parameter tuning for the four protein Cascade system. Relative error quantification over: (a) increasing number of samples per time point, (b) increasing sampling time difference $[dt]$ between clouds, (c) increasing number of spatial test-functions M_1 , (d) increasing number of temporal test-functions M_2 for different variance of clouds of samples (i.e. different stochastic noise coefficient σ). The optimal parameters that are set constant while varying the others as shown in (a)-(d) are $NoS = 400$, $dt = 0.5$, $M_1 = 25$, $M_2 = 15$ for this example of stochastic noise coefficient $\sigma = 0.01$ and errorbars are over 6 i.i.d runs. We deduce that more samples per sampling time point improve the integral estimations of Equation (3.1), resulting in lower relative error as shown in (a). In (b) we see that as the sampling time difference between the clouds of data is increased more than 0.75 time units for this system, successful recovery of \hat{A} is not feasible. (c) demonstrates that by employing more B-splines, their support is decreased and as a consequence the relative error increases. The inferred solution \hat{A} collapses (relative error sharply approaches 1) when the support of the B-splines is much smaller (over 4 times smaller) than the variance of each propagating cloud. Increasing values of stochastic noise σ , resulting to wider clouds, further verify this result. Temporal test functions parameter shown in (d) is less sensitive wrt the relative error. The optimal value of Fourier modes to be used is 15 for this example clouds sampling time difference set at $dt = 0.5$ time units.

Moreover, the support (or width) of each B-spline should be equal or greater than the variance of each cloud in order for the algorithm to track their evolution over time. In other words, a cloud captured by only one B-spline at a given time point once, does not carry enough information that can be subsequently projected to temporal test functions and constitute a useful projected pdf. In this example, where the variance of the steady state clouds of samples is around 0.1 ($\sigma = 0.01$), the relative error spikes to 1 (cyan line) when 40 B-splines are used with 0.035 spatial units support. Increasing values of stochastic noise σ , resulting to wider clouds, require wider B-splines hence smaller M_1 .

The number of temporal test functions M_2 (Fourier modes) used, is related to encoding spatially projected information over time and depends on the curvature of the clouds over time and the placement of nodes of spatial test functions. Faster changes in time (steep curvature) require higher frequency sinusoidal functions. In Figure 7(d), by employing three temporal test functions M_2 , only the low frequency changes are identified. On the other hand, higher frequency sinusoidal functions encode noise thus deteriorating the relative error. This limitation of constantly improving the relative error by using more sinusoidal over fixed sampling rate [rate is determined directly by dt and its variability by M_1], is related to the Nyquist–Shannon sampling theorem in conjunction with the sampling time difference used in Figure 7(b). Although this hyper-parameter is less sensitive with respect to the others, we conclude that the determination of M_2 is problem specific and tuned in accordance to M_1 , with respect to the metric chosen. More detailed experiments indicating the inter-dependence of these parameters are provided in the supplementary material (S.M.5).

4.3. Biochemical protein reaction network inference using Mass cytometry data. We proceed and evaluate our proposed methodology on real publicly available mass cytometry

data [17]. Mass cytometry cell analysis techniques are important for understanding cellular responses (stimuli from other cells, signals etc) by measuring tens of interacting proteins in each cell simultaneously (predefined times), over millions of cells. Given the high resolution it is expected to become a standard technique in medical sciences in the near future. Reconstructing the pathway upon activation (ordered relation and intensity between proteins) is a non-trivial task because only a few proteins inside the cells are measured and on top of that many interfering mechanisms with different rate are also occurring. Considering the above, it is very hard to reconstruct directly the complete system of interactions. However, network reconstruction would be more successful if restricted to subnetworks. The abundance of each protein can be described as a stochastic process affected by the abundance of other proteins, so the underlying model is chosen to be an SDE for each one. Using our Fokker Planck formulation, the propagating density of abundances in the form of population data, is a novel approach to this statistically limited data regime. Next, we focus on a subnetwork of four and eight proteins (supplementary). Our findings are compared qualitatively against other studies [17, 22] and from the KEGG database, since the exact interactions mechanism are unknown.

Experimental data belong to the population of naive $CD4^+$ regulatory T-cells and the activation cocktail which stimulate the receptors CD3/CD28 were applied. We focus on the subnetwork containing proteins pCD3z, pSlp76, pErk and pS6, downstreaming the signal in this order (cascade). The mass-cytometry measurement times are closer at earlier times, where dynamics prevail though scarce as one can see in Figure 8 (upper left).

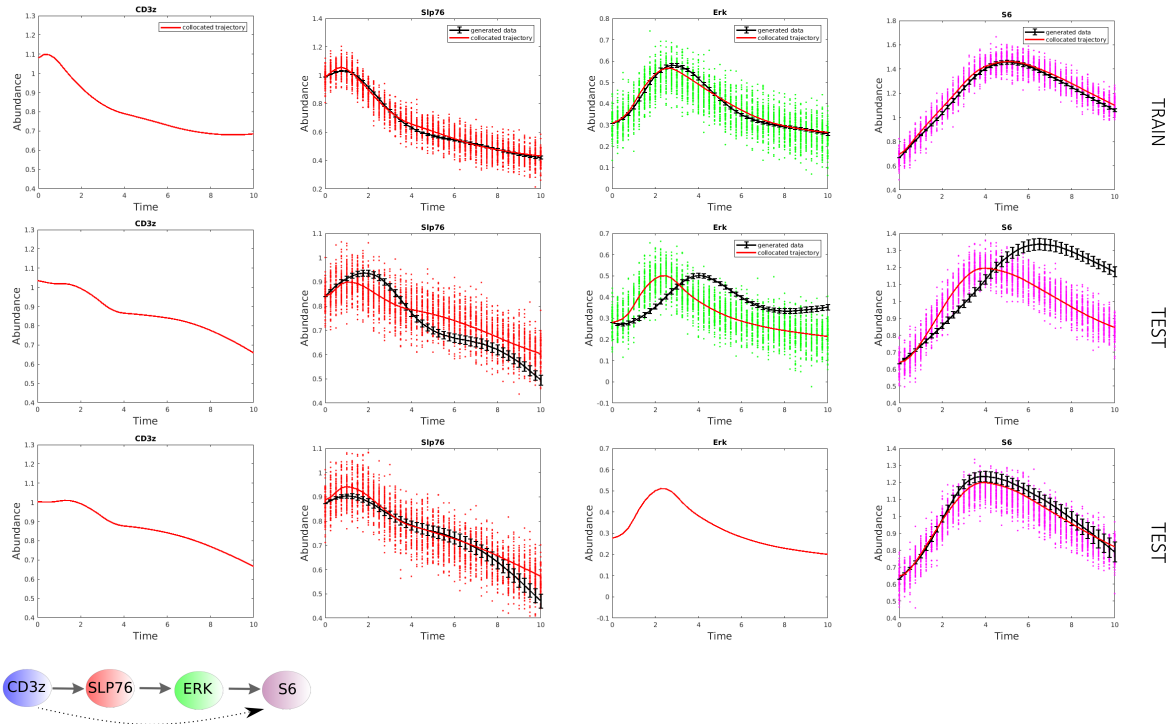
In the data set under study and mass cytometry data sets in general, sampling times are scarce resulting to poor dynamical information. Hence the algorithm would not be able to deduce the underlying interactions correctly without more frequent temporal measurements (as shown in the supplementary material), as there exist multiple dynamics that could give rise to the measured distributions or in other words, multiple possibilities for the underlying mechanisms (see [34] for a thorough explanation on inference limitations on single-cell data). The current framework assumes Gaussian stochastic noise over each cloud, which does not hold upon inspection of the histograms. Variable variance as time progresses is another peculiarity of this data-set, as our current framework assumes constant σ . Last, smoothing out the dynamics of the propagating distributions is desirable in this context of: very limited measurement times, no additional interventions and high measurement noise of unknown number of unmeasured variables. For these reasons, we propose re-simulation of the input population data, by the collocation method (details in the supplementary and previous our publication [22, 23, 24]) and all the analyses in this subsection are based on re-simulated data. The collocation method, is a regularized least-squares minimization, taking account of the variance of each cloud of samples, along with their relative distance in time and thus provides a well-informed time-series (or multiple time-series in case of multimodality) on which population data are simulated. Re-simulation is vital for obtaining a meaningful solution under this particular regime, taking account of the advantages and limitations of PDL as discussed in Subsection 4.1 and Subsection 4.2. A more advanced method for curve fitting time-course gene expression data, along with a review on this subject can be found in [18], though the collocation method is satisfactory for our demonstrations.

We remark that by construction, there is no need of random term to be included in the inference, thus $\Sigma = 0$ in Equation (2.4). Nevertheless each cloud of samples is based on

a Gaussian distribution resembling measurement noise and the theoretical deductions from Equation (2.4) up to Equation (D.6) hold, known under the name of Liouville equation.

Despite the fact that the complete biochemical network is probably nonlinear with respect to the variables, the assumed model for inference is linear $\frac{dX}{dt} = AX$, similar to subsection 4.2 (for $\Sigma = 0$). The linear model is sufficient for this low dimensional\single maximum paradigm and at the same time, the associated connectivity matrix A encodes only the direct causal interactions between the variables. Another inherent difficulty on the inference of this example is: a) the measurement error associated with machine errors, assumed to be additive and b) uncertainty error due to the fact that each measurement comes from a different cell and each cell has different concentrations of the measured quantities.

4.3.1. External forcing as prior knowledge: Four-protein pathway. A major modelling assumption of the formalism is that the modelled system is closed. Intuitively this means that only the variables considered, account for changes on each other over time (where non-modeled or stochastic forces are on top of these changes, casting the distributional clouds). On the contrary, this does not hold true for a real biochemical pathway where the proteins are sequentially converted to the next and in which we merely focus on a fraction of the variables. Considering all the aforementioned, we add driving protein CD3z to the inference, infer CD3z, use its data though never use it to generate trajectories for that particular particular variable. In this way we extract information from this driving variable, improve the inference of the other three, at the cost of not having a meaningful SDE describing CD3z (see demonstration in supplementary). PDL returns an SDE for CD3z that is good fit, though not meaningful as based on the others. The reason for the problematic inference for this variable arises because a combination of the linear dictionary terms, starting from an initial abundance distribution $p_0(X)$, is used to describe the curvature of the sole driving variable, *in a closed system*. Hence additional interactions of the modelled variables are devised to account for the *non-monotonic* behavior of CD3z, which in principle is regulated by unmeasured non-modeled variables. Using but not inferring CD3z consists prior knowledge to the system because from a biological point of view, the CD3z protein lies in the cell surface being one of the gatekeepers of T-cell activation (signal transduction) [6].



protein	CD3z	SLP76	Erk	S6
$\ X_{coll} - X_{gen}\ _2$ (train)	0	0.026	0.047	0.029
$\ X_{coll} - X_{gen}\ _2$ (test)	0	0.066	0.33	0.28
$\ X_{coll} - X_{gen}\ _2$ (test)	0	0.035	0	0.072

Figure 8. Population data (dots) of four protein $CD3z$, $SLP76$, Erk and $S6$ abundances, based on re-simulated data as explained in subsection 4.3. (first row panels) The average generated trajectories based on inferred \hat{A} matrices of 25 training sets are shown in black solid lines with error-bars, and their average L_2 distance from the collocated trajectories (red solid lines) is shown in the table. The driving protein $CD3z$ is given as prior knowledge as mentioned in the main text. We used a quadratic dictionary which results to a more accurate \hat{A} in comparison with the linear, based on the L_2 distance, although the pairwise associations between variables remain (graph). The difficulty of this example is finding a model that is minimally complex (low order terms) and at the same time capture the dynamics (curvature) and explain the interactions (qualitatively as graph and quantitatively as equations). The graph shows the inferred relations based on the structure of \hat{A} and the dashed edge $CD3z \rightarrow S6$ is a false positive that is not found in the bibliography, possibly an artifact of limited temporal measurements. We conclude that the inferred models \hat{A} predict the behaviour of the input data satisfactorily. (second row panels) Use of \hat{A} matrices from training set on test set of another activation-dosage (laboratory test), in order to estimate performance. Our assumption is that the underlying mechanisms remain the same over this protein subnetwork. We see that there is partial transferability of the inferred model, probably due to the difference of the driving protein $CD3z$ affected by unmeasured proteins. Nevertheless, none of the trajectory deviates and qualitatively we claim that the underlying mechanism is the same in both data sets. (third row panels) Extra prior knowledge on Erk further improving the test set fitting, indicating the accuracy of our models and the limited knowledge of unmeasured proteins. Further experiments are included in the supplementary material SM1, SM7.

As we already mentioned, higher order dictionaries can be more precise though their use in interpreting the interactions is more complex. In fact, low sample sizes or infrequent

sampling, coupled with high order dictionaries run the risk of overfitting. In order to be able to achieve more precise fitting over the linear dictionary (shown in supplementary) and retain interpretability with respect to interactions, we added quadratic terms of the form $x_1^2, x_2^2, x_3^2, x_4^2$ to the dictionary [Figure 8](#). Depending on the application, there is a trade-off between model complexity and interpretability.

[Figure 8](#) shows the four-protein pathway, where the driving variable CD3z data is used for the inference of the rest; proteins Slp76, Erk and S6. In this way we use the past of the CD3z for the future trajectory of the SLP76, Erk and S6. Random subsampling (of size 800 samples per time point) of the mass-cytometry data, result to slightly different inferred dynamical systems or connectivity matrices \hat{A} . Based on those inferred matrices, we generate data trajectories using a numerical integration scheme (4-th order Runge-Kutta), starting from an initial configuration p_0 deduced from the population data at $t = 0$. As it is evident from the [Figure 8](#) (first row panels), the generated trajectories based on the inferred systems are in accordance with the input population data, capturing the minima correctly. Examples of these, sequentially dependent systems, are sensitive to lagged or imprecise derivative estimations, because the errors are accumulated down the pathway. Next we try to assess the inferred matrices \hat{A} on experimental data (test set) coming from another activation, corresponding to a different dosage. We do not know in advance if we can capture the dynamics correctly, although we expect that the underlying mechanisms should remain the same, with a different initial distribution p_0 . [Figure 8](#) (second row panels) shows a satisfactory (non-divergent) fit, not being able to capture the maxima exactly. This might hold for a number of reasons. First and foremost, we focus on the modelling of a subnetwork and there might be other, unmeasured mechanisms due to the different dosage. Secondly, we chose a quadratic polynomial that best fits the input data, though it might be less transferable for this dataset. Third, the accumulated error in this cascade, builds on the last protein S6. We further add protein Erk as prior knowledge and conclude to an improved estimation for the dynamics of the other proteins of the test set ([Figure 8](#) last row panels). This implies that there exist hidden mechanisms, in the form of unmeasured proteins, affecting this four protein cascade and one of the assumptions we make is that there is no confounding ([Appendix A](#)). A similar conclusion for mass cytometry data on the differentiation of fibroblast cell line beyond a time point, is discussed in [\[30\]](#).

We show in the supplementary material that a linear dictionary is less accurate than a quadratic dictionary but slightly more transferable. Results on a bigger protein network are included.

5. Discussion. Our work lies in the identification of the underlying system of differential equations based on spatio-temporal data. We have presented a new robust algorithm, PDL, for the inference of stochastic dynamical systems based on population (or time-course) data. This work builds on our previous framework [\[22\]](#), extending from trajectorial (or time-series) data to propagating distributions, with the deduction of the Fokker-Planck formalization. To the best of our knowledge, this is the first approach in deriving both the unknown drift and diffusion equation terms from population data, without transforming it into trajectories instead. The latter pdf evolution can be multimodal in principle, capturing meta-stability of the underlying unknown system and this is our major contribution to the field. In the synthetic

example cases, perfect identification of the stochastic dynamics was achieved. In addition to other methods that capture the deterministic parts of SDE's (terms comprising the gradient of a potential) provided that the dynamics have reached a steady-state, we were able to recover the diffusion coefficient of SDE's (noise term). A limitation of the current SDE model, not the PDL framework, is the assumptions of i) the diffusion coefficient in the noise term of the SDE being constant over time, ii) the Brownian motion random term being normally distributed. Nevertheless, these assumptions can be overcome, as shown in the main text, by re-simulation of the data with an equivalent data set. Moreover, deduction of an extended form of the FP equation for multiplicative Brownian motions can be derived analytically for these cases.

The cornerstone of our work, is the weak space formulation of the problem, transforming it to an atemporal one while preserving the unknown coefficients. In this way, we gain robustness against measurement noise, scalability to higher dimensions and longer times provided that an appropriate choice of test-functions is made. Along with test-functions, an appropriate choice of dictionary is crucial for solving this inverse problem. A dictionary lacking major terms (low expressive power) of the unknown equation cannot always be compensated by higher order terms, whereas a very rich dictionary (especially in the low sample or high measurement noise regimes) can induce spurious correlations and make sparse regression harder. There is no universal solution to this challenge, as it requires prior intuition on the dynamics of the data set in order to provide the algorithm with explanatory features.

The PDL algorithm, correctly identified the non-linear double-well system, having the intrinsic difficulties of bi-modality, different diffusion coefficients and different equilibration times. The algorithm is designed such that, additional data in the form of different initial conditions or interventions on variables, can be incorporated (in a straightforward manner on top of previous computations) and bolster its inference capabilities. Towards the same direction is the direct supply of prior knowledge, in case we have strong evidence of some dictionary terms being present. The majority of the algorithms of ODE's or PDE's are based on the approximation of temporal or spatial derivatives by a numerical scheme like finite differences, which are very sensitive to noise of "unclean" data. This fact requires smoothing techniques in order to produce reasonable approximations, though PDL shifts this burden to the (smooth) test-functions via the weak formulation.

In this current form, the algorithm requires the propagating distributions (clouds) to be measured frequently, in order to be captured by the spatial test functions and subsequently, by the temporal test functions. This might prove to be a limitation in specific applications of the algorithm, nevertheless we proposed the collocation method as a practical solution. Although smoothing in time is avoided, we still need temporal information (either in the form of frequent measurement or with additional interventional data) in order to disambiguate the alternative dynamics, depending on the smoothness of the evolving clouds. We strongly believe that this limitation can be alleviated with a more sophisticated choice of data-driven test functions, which is under investigation. PDL scales well with increasing number of samples (used in the integral estimators), although the current implementation is restrained by the variable with the biggest range, which might prove slow for systems with unbalanced relative magnitudes of variables.

Application to mass-cytometry data, upon inspection making realistic assumptions on the interactions, concluded to results supported by the literature. Preprocessing by re-simulation

of the population data was mandatory due to uneven, distant measurement time-points along with non-Gaussian skewed pdf's swamped in measurement noise, which violated the algorithm assumptions. The inferred subnetworks of interacting proteins included some additional interactions, though it was expected for this low-informative data set and our dictionary choice.

Appendix A. Model, Notation and Assumptions.

The general form of a system of SDE's reads:

$$(A.1) \quad \begin{aligned} dX_t &= a(X_t, t)dt + b(X_t, t)dB_t \\ X_t \in \mathbb{R}^N, \quad a(X_t, t) &: \mathbb{R}^N \times \mathbb{R}^+ \mapsto \mathbb{R}^N \\ b(X_t, t) &: \mathbb{R}^N \times \mathbb{R}^+ \mapsto \mathbb{R}^{N'} \\ B_t \in \mathbb{R}^{N'} &\text{ is } N'\text{-dimensional Brownian motion} \end{aligned}$$

where the first term on the r.h.s. of Equation (A.1) is the deterministic term whereas the second term is the diffusion (random forcing). $a(X_t, t)$ is a vector field called *drift* and $b(X_t, t)$ is a matrix field called the *diffusion* coefficient of the process X_t . B_t constitutes an N' -dimensional Brownian motion, so their product acts as a random force on top of the deterministic counterpart, which is normally distributed, thus not making the deterministic dynamics diverge in later times. Intuitively, the derivative of a Brownian motion dB_t can be understood as a continuous-time zero-mean white noise with variance one.

Assumption 1: The random term describes all the **latent variables** (unknown) acting on the variable being modelled. In case where no latent variables are present, the model reduces to an ODE (or PDE) where the deterministic term $a(\cdot, t)$ takes over.

We choose an appropriately rich dictionary of functions (in other context termed dictionary atoms) $\psi_q(X(t)) : \mathbb{R}^N \mapsto \mathbb{R}, q = \{1, \dots, Q\}$ which serve as basis functions for the drift term.

Assumption 2: The n -th deterministic drift term $a(X_t^n, t)$ can be written **exactly** as a linear combination of the dictionary atoms by:

$$(A.2) \quad a(X_t^n, t) = \sum_{q=1}^Q a_{n,q} \psi_q(X(t))$$

Note that in general, $\psi_q = \psi_q(X(t))$ meaning that we include non-linear functions such as $X_n^2(t), \cos(X_n(t)), X_n X_{n'}$ etc as well. The constants $a_{n,q}$ make up the connectivity matrix $A \in \mathbb{R}^{N \times Q}$ of unknown coefficients to be determined later and determines the interactions between variables X .

Assumption 3: Time-invariant diffusion coefficient of each process X_t^n

$$(A.3) \quad b(X_t^n, t) = \text{constant over time} = \begin{bmatrix} \sigma_1 \\ \sigma_2 \\ \vdots \\ \sigma_N \end{bmatrix}$$

In practice, time invariance means that unmeasured variables do not affect the process X_t^n in a different manner throughout the time measurements. More complex forms of diffusion could better reflect reality though this simplification is sufficient for our modelling.

The covariance matrix of the diffusion of [Equation \(A.1\)](#) accounts for interactions between the unknown variables and is given by:

$$(A.4) \quad \Sigma(\mathbf{x}) = \sigma^T(\mathbf{x})\sigma(\mathbf{x}), \quad \mathbf{x} \in \mathbb{R}^N, \Sigma \in \mathbb{R}^{N \times N}$$

Assumption 5: The covariance matrix is diagonal:

$$(A.5) \quad \Sigma = \begin{bmatrix} \sigma_1^2 & 0 & \dots & \\ 0 & \sigma_2^2 & 0 & \\ \vdots & & & \\ & & \dots & \sigma_N^2 \end{bmatrix}$$

This implies that there are **no latent confounders** in the dynamics. Only latent variables affecting **one** system variable X_t^n .

Appendix B. Measurement Data.

B.1. 1-Dimensional SDE. We define L objects $\{O\}_{l=1}^L$ that propagate in time, where O_l is a specific item i.e. protein concentration and $L \gg 1$. We further assume that time is continuous and each object value at time t : $O_l(t)$ is given by a stochastic process whose SDE is given by:

$$(B.1) \quad d(O_l)_t = \mu((O_l)_t, t)dt + \sigma(O_l, t)dW_t$$

where the first term on the r.h.s. is the (deterministic) drift term whereas the second term is the diffusion (random forcing), as in [Equation \(A.1\)](#).

B.2. Mass Cytometry measurements. Instead of the 1-Dimensional value each object $O_l(t)$ acquires in time, we get P *measured* values, at predefined measurement times $t_k \in \{t_1, t_2, \dots, t_K\}$, each contaminated with measurement error. Let variable X measure the objects and S_t be the set of those measurements at time t_k

$$(B.2) \quad S_{t_k} = \{x^p, \quad p = 1, \dots, P_{t_k}\}$$

$$(B.3) \quad x_k^p = X(O_l(t_k)) = O_l(t_k) + \text{msnt_err}$$

Assumption 6: $\text{msnt_err} \sim \mathcal{N}(0, \sigma_{\text{msnt}})$, which is a reasonable assumption for mass cytometry data and measurement data in general provided no bias along measurements. In the following synthetic examples, σ_{msnt} can be chosen appropriately small, so that noise doesn't flatten (dominate over) the distribution of samples per time-point. As we later explain, this error is incorporated in the latent variables, though **from this point on, we consider as data, only the measurements** $x_{n,k}^p$ (n indicating variable index).

Note: We randomly pick P out of the L in total, on every non-repeated measurement time-point t_k . Each measurement destroys the object, so there cannot be $X(O_l(t_{k+1}))$ after $X(O_l(t_k))$. Instead we might measure $X(O_{l+7}(t_{k+1}))$ for instance, where O_{l+7} has not been measured in $\{t_i\}_{i=1}^k$. Formally

$$\{O_{t'}\} \cap \{O_{t''}\} = \emptyset, t' \neq t''$$

This does not pose a problem, as we are interested in the distribution of the iid measured objects as a set (distribution at specific time point) and not in each individual object. The data we will be considering from this point on, can be written in vector form as:

$$(B.4) \quad S = [x^{(1)}(t_1), \dots, x^{(1)}(t_K), \dots, x^{(P)}(t_1), \dots, x^{(P)}(t_K)]$$

Assumption 7: The measured objects $x^{(p)}$ are described by stochastic processes, although there is no one-to-one correspondence along measurement times. We will use this modelling assumption to formulate the time evolution of $S_{t_k} = \{x^{(p)}(t_k), \dots, x^{(p)}(t_k)\}$ later on and the generalization to N dimensions $S_{t_k}^N$.

We can now think of X as a stochastic variable, having a density comprised of P samples, on every time point t_k , where these samples come from P *realizations* (termed trajectories) of the same underlying SDE.

There are two major categories of temporal data depending whether the same object (variable) is repeatedly measured or not; time series and time-course (or population) data. For the case of time series data, each object is measured sequentially over time at predefined sampling time-points. On the contrary, non-repeated measurements or time-course data, measure a different object at each time instant. This might be the case when the object is destroyed along the measurement process, as for instance, in mass cytometry (see discussion above), requiring re-initialization for data acquisition at later times. However, it is assumed that (under the same experimental conditions) all measured objects are drawn from the same unknown distribution.

Appendix C. Fokker Planck: general form.

The FP equation, for the general stochastic process [Equation \(A.1\)](#), is a $N+1$ dimensional parabolic PDE given by:

$$(C.1) \quad \partial_t p(\mathbf{x}, t) = - \sum_{n=1}^N \partial_{x_n} \{a_n(\mathbf{x}, t)p(\mathbf{x}, t)\} + \frac{1}{2} \sum_{n_1, n_2=1}^N \frac{\partial^2}{\partial x_{n_1} \partial x_{n_2}} \{D_{n_1 n_2}(\mathbf{x}, t)p(\mathbf{x}, t)\}$$

$$(C.2) \quad D_{n_1 n_2}(\mathbf{x}, t) = \frac{1}{2} \sum_{k=1}^{N'} b_{n_1, k}(\mathbf{x}, t) b_{n_2, k}(\mathbf{x}, t)$$

with initial condition $p(x, 0) = p_0(x)$. Upon the assumptions on the drift and noise terms ([Appendix A](#)), the special case considered in this manuscript is given by [\(2.4\)](#).

Appendix D. Weak formulation.

Equation (3.1) can be written as

$$(D.1) \quad \begin{aligned} \langle \phi_m(\mathbf{x}, t), \partial_t p(\mathbf{x}, t) \rangle &= - \sum_{n=1}^N \langle \phi_m(\mathbf{x}, t), \partial_{x_n} \{a_n^T \psi(\mathbf{x}, t) p(\mathbf{x}, t)\} \rangle \\ &+ \frac{1}{2} \sum_{n=1}^N \langle \phi_m(\mathbf{x}, t), \partial_{x_n x_n} \{\sigma_n^2 p(\mathbf{x}, t)\} \rangle, \quad m = 1, \dots, M \end{aligned}$$

with the $\langle f, g \rangle = \int_0^T f(t)g(t)dt$ denoting the inner product between functions f and g in the $L^2(\mathbb{R}^{N+1})$ function space.

We proceed with integration by parts and after straightforward calculations:

$$(D.2) \quad \begin{aligned} &\int_{\mathcal{D}} \phi_m(\mathbf{x}, T) p(\mathbf{x}, T) d\mathbf{x} - \int_{\mathcal{D}} \phi_m(\mathbf{x}, 0) p(\mathbf{x}, 0) d\mathbf{x} - \int_0^T \int_{\mathcal{D}} \partial_t \{\phi_m(\mathbf{x}, t)\} p(\mathbf{x}, t) d\mathbf{x} dt = \\ &\sum_{n=1}^N \sum_{q=1}^Q a_{nq} \int_0^T \int_{\mathcal{D}} \partial_{x_n} \{\phi_m(\mathbf{x}, t)\} \psi_q(\mathbf{x}) p(\mathbf{x}, t) d\mathbf{x} dt + \frac{1}{2} \sum_{n=1}^N \int_0^T \int_{\mathcal{D}} \sigma_n^2 \partial_{x_n x_n} \{\phi_m(\mathbf{x}, t)\} p(\mathbf{x}, t) d\mathbf{x} dt \end{aligned}$$

where we assume that the distribution is zero on the boundary $p(\mathbf{x}, t)|_{\partial \mathcal{D}} = 0$ for all t . It is apparent that by applying the weak formulation, the derivatives are "shifted" to the test functions ϕ_m , which is one major advantage of our modeling approach.

As one can see, the integrals are N -dimensional as the variables $\{X^n\}_{n=1}^N$ are coupled in general. In the following, we define these spatio-temporal functions as:

$$(D.3) \quad \phi_m(\mathbf{x}, t) := \bar{\phi}_{m_1}(\mathbf{x}) \tilde{\phi}_{m_2}(t)$$

meaning that space $\bar{\phi}_{m_1}$ and time $\tilde{\phi}_{m_2}$ have different functional forms and $m_1 \in \{1, \dots, M_1\}$, $m_2 \in \{1, \dots, M_2\}$, $M_1 M_2 = M$. We choose test functions in a way that their form is able to capture the data heterogeneity, form and time-scales as we discuss later on. Moreover this is why their functional form are different in principle, though we could use the same family of functionals.

On top of the choice of (D.3), we proceed with the simplification regarding the (de)coupling of the spatial variables:

$$(D.4) \quad \bar{\phi}_{m_1}(\mathbf{x}) \approx \bar{\phi}_{m_1}(x_1) \dots \bar{\phi}_{m_1}(x_N)$$

though the variable **interactions are incorporated in the dictionary atoms** because the drift term $\mathbf{a}_n \Psi(X)$ term constitutes of $Q \geq N$ components (for a linear dictionary $\Psi(X(t)) = X(t)$ and $Q = N$).

Superposition assumption: We assume that the unknown complex distribution $p(\mathbf{x}, t)$ can be written as a linear combination of simple, "appropriately chosen", spatio-temporal test functions:

$$(D.5) \quad p(\mathbf{x}, t) = \sum_{m_1} \sum_{m_2} d_{m_1, m_2} \tilde{\phi}_{m_2}(t) \prod_n \bar{\phi}_{m_1}(x_n)$$

We proceed with Equation (D.2), for $n \in \{1, \dots, N\}$ variables in total, so for the n -th component and m_1 -th, m_2 -th test functions we get:

(D.6)

$$\begin{aligned} & \int_{\mathcal{D}_n} \bar{\phi}_{m_1}(x_n) \tilde{\phi}_{m_2}(T) p(x_n, T) dx_n - \int_{\mathcal{D}_n} \bar{\phi}_{m_1}(x_n) \tilde{\phi}_{m_2}(0) p(x_n, 0) dx_n - \int_0^T \int_{\mathcal{D}_n} \bar{\phi}_{m_1}(x_n) \partial_t \tilde{\phi}_{m_2}(t) p(x_n, t) dx_n dt \\ &= \sum_{q=1}^Q a_{nq} \int_0^T \int_{\mathcal{D}} \partial x_n (\bar{\phi}_{m_1}(x_n)) \tilde{\phi}_{m_2}(t) \psi_q(\mathbf{x}) p(\mathbf{x}, t) d\mathbf{x} dt + \frac{\sigma_n^2}{2} \int_0^T \int_{\mathcal{D}_n} \partial_{x_n x_n} (\bar{\phi}_{m_1}(x_n, t)) \tilde{\phi}_{m_2}(t) p(x_n, t) dx_n dt \end{aligned}$$

where we have $N \times M$ integral equations in total. Note that the first two integrals in the l.h.s. depend on the population data of $X(t_1)$ and $X(t_K)$ so we consider them as constants $C_{m_1, m_2, n}$ computed once.

Appendix E. Integral Estimators. Suppose that we fix time $t = \tau$ and let x_i be drawn from $p(x, \tau)$, as is the case with population data. Then for any function $f(x) : \mathbb{R}^N \mapsto \mathbb{R}$ we approximate:

$$(E.1) \quad \mathbb{E}_{p(x; \tau)}[f(x)] = \int_{\mathcal{D}} f(x) p(x; \tau) dx \simeq \frac{1}{P} \sum_{i=1}^P f(x_i)$$

where P is the number of samples considered. Also, we approximate the time integral on the discretized time domain $\{t_1 < t_2 < \dots < t_K = T\}$ using the standard numerical analysis trapezoidal rule on $f(x, t) : \mathbb{R}^N \times \mathbb{R}^+ \mapsto \mathbb{R}$:

$$(E.2) \quad \begin{aligned} \mathbb{E}_{p(x, t)}[f(x, t)] &= \int_0^T \int_{\mathcal{D}} f(x, t) p(x, t) dx dt \\ &\simeq \frac{1}{2} \sum_{k=1}^{K-1} \left(\int_{\mathcal{D}} f(x, t_{k+1}) p(x, t_{k+1}) dx + \int_{\mathcal{D}} f(x, t_k) p(x, t_k) dx \right) (t_{k+1} - t_k) \end{aligned}$$

Appendix F. Minimization problem. In the ideal case where the number of rows (test functions) M is equal to the number of columns (dictionary atoms) Q in matrix Ψ , one could possibly solve the system directly and recover the correct coefficients provided that the noise in the data has not affected the condition of matrix Ψ . In principle though, the resulting systems are over-determined because we use a large number of test functions and a broad family of potentially useful dictionary atoms, and a least-squares type minimization of the form $\min \|Z - \Psi a\|$ over a , does not have a sparse solution but a full (dense) one. Formally

$$(F.1) \quad \min_a \|Z - \Psi a\|_2^2, \quad \text{with solution} \quad \hat{a} = (\Psi^T \Psi)^{-1} \Psi^T Z$$

In practice, a dense solution means that there is a high correlation of the available candidate features (columns of Ψ) as a result of noise in the data (ill-conditioned matrix Ψ) and sparse regression is preferable. To achieve this, a minimization problem with penalization is solved instead:

$$(F.2) \quad \min_a \|a\|_0 \quad \text{subject to} \quad \|Z - \Psi a\|_2 \leq \epsilon,$$

which uses the L^0 norm over the minimization, where $\|a\|_0$ is the number of non-zero elements in a and ϵ is the regression error. This is a non-linear, non-convex optimization problem (NP-hard) and the solution space grows exponentially with the size of a making it computationally intractable. A usual approach is to relax the norm in the objective function and solve the convex L^1 least-squares minimization problem or the L^1 -regularized form:

$$(F.3) \quad \min_a \left(\frac{1}{2} \|Z - \Psi a\|_2^2 + \lambda \|a\|_1 \right),$$

where sparsity is enforced by the L^1 norm and controlled by the positive Lagrange multiplier λ [26]. In other words, λ balances complexity and sparsity of the solution and an approximation algorithm solving (F.3) is LASSO [32]. See [16] for a two step modified Lasso suited for high dimensional, multiscale stochastic (unary/binary) reaction networks using time series data having intrinsic uneven noise. Our modelling assumption is that the underlying dynamics are governed by a few terms, which in mathematical terms translates in sparsity of the solution of (3.5).

We note that despite its computational advantages, the least-squares approach in system identification usually produces a “full” solution where each component of a is nonzero despite the true structure being sparse, making inference algorithms sensitive to noise and under-sampling. A computationally demanding alternative though robust against noise and outliers (avoiding over-sparsity) is the Entropic Regression system identification [2]. We demonstrate robustness of our proposed algorithm against outliers in the supplementary material provided. One can combine the least-squares formulation with thresholding (either iterative [5, 4] or not, hard [5, 20] or soft [4]) and conclude to a desirable, sparse solution.

Hyper-parameter tuning is important, because an excessively sparse solution will under-fit the data whereas a nearly full solution will over-fit. The chosen criterion for OMP parameter tuning is the Bayesian Information Criterion (BIC) penalizing model complexity (more terms in the solution) and specifics can be found in the Supplementary. We remark that the sparse optimization problem penalizes the magnitude of the coefficients directly, so in order to avoid inclusion/exclusion of a feature whose vector magnitude differs substantially from the others, we normalize each column ψ_q of Ψ by its L^2 -norm.

Appendix G. System interventions: additional datasets from variable perturbations. It is usually the case that multiple datasets of the *same underlying mechanism* are given as input. A significant attribute of the USDL methodology is the framework of handling additional data, of the same set of variables and sampling times. Let us assume for illustration purposes that we simulate a known differential equation multiple times while perturbing its variables and generate datasets, each containing many trajectories. These datasets can be categorized in two types: i) activation: starting the simulation from a different initial configuration, eventually evolving to a steady or equilibrium state, and ii) inhibition: neutralization of the effect of a specific variable over time.

Exploration of the phase space, through additional data, results in rich dynamical information as input to the inference problem, narrowing down the possible solutions to the minimization problem discussed in subsection 3.2.1. In other words, additional data make the unknown system more identifiable. On the contrary, as the number of state variables

increases, very large sample sizes are required for successful inference, which for biological laboratory experiment measurements cannot be available, though experimental perturbations can be performed instead. These type of variable perturbations can be incorporated through interventions [22]. Collectively, i) and ii) constitute interventions on the underlying system. Each different activation intervention r , results to a new SLE of the form of Equation (3.5) (remark that we omit species index n) such that:

$$(G.1) \quad Z^{(r)} = \Psi^{(r)} a^{(r)}$$

where the unknown $a^{(r)}$ vector should have been determined independently. On the contrary, we merge the weak space projected data into a larger SLE, so in matrix form we end up with Figure 9: where a is determined over all activations with a single call of the feature selection

$$\begin{bmatrix} Z^{(1)} \\ Z^{(2)} \\ \vdots \\ Z^{(R)} \end{bmatrix} = \begin{bmatrix} \Psi^{(1)} \\ \Psi^{(2)} \\ \vdots \\ \Psi^{(R)} \end{bmatrix} a$$

Figure 9. R activation interventions in matrix form (for the n -th variable)

algorithm. In the examples in Section 4 we used activations, though we refer the reader to the supplementary material for the derivation of inhibitions for the SDE setup, similar to the ODE ansatz [22].

- Appendix H. Algorithm limitations.**
1. Might be slow for variables having wide range being captured by spatial test functions, though current matlab version is parallel and scales well.
 2. Partial parameter setting based on fitting to average trajectories of the input data. Data driven test functions and automatic algorithm hyper-parameter estimation (M_1, M_2 , feature selection stopping criteria) is under development.
 3. Requires relatively short sampling times (w.r.t. the fastest dynamics) for adequate time-derivative component estimation [not particularly short, as short as a finite difference scheme would require]. Tackled with data resimulation (constrained smoothing or collocation method).
 4. Requires Gaussian constant-variance noise. Tackled with resimulation of the data.
 5. Depending on the identifiability or complexity of the system, it might require multiple interventions (activations/inhibitions) in order to gain insight from richer dynamics.

Appendix I. Notation.

Acknowledgments. We would like to thank Georgios Papoutsoglou for his helpful comments. This work was funded by the European Research Council under the European Union's Seventh Framework Programme (FP/2007-2013) / ERC Grant Agreement n. 617393.

REFERENCES

table containing common acronyms, terms and mathematical notation	
FP	Fokker Planck equation
SDE	Stochastic Differential Equation
PDL	Population Dynamics Learning
X_t^n	n -th variable which is a stochastic process
X_t	vector of variables (stochastic processes) which follow SDE's
$X(t)$	set of data points at time t of vector of variables X_t
$\mathbb{P}(X_t, t)$	unknown probability density function describing evolution of variables X_t
$p(\mathbf{x}, t)$	value of the pdf for all data \mathbf{x} at time t that is $X(t)$
P	number of data points measured per time point
S	set of all data points over all time points (possibly over multiple interventions)
Q	number of dictionary atoms
$\psi(x)$	vector of symbolic functions of dictionary items
$\psi_q(x)$	q -th dictionary item
Ψ	data matrix over dictionary items (all timepoints)
$\phi_m(x, t)$	m -th test function (constructed feature)
$\bar{\phi}(x)$	spatial test function
$\tilde{\phi}(t)$	temporal test function
M	number of test functions in total
Z	matrix containing time derivatives projected to Weak Space
$\tilde{\Psi}$	matrix containing projected dictionary items to Weak Space
$\tilde{\Psi}_n$	n -th column of matrix Ψ for n -th variable
W	matrix containing projected diffusion term to Weak Space
A	unknown matrix of constants defining coefficients of the solution
\mathbf{a}_n	vector of n -th row of A defining dictionary coefficients of that variable
Σ	(diagonal) covariance matrix of diffusion coefficients of the solution
\mathcal{D}	subspace of \mathbb{R}^N where data are measured
OMP	Orthogonal Matching Pursuit learning algorithm
rr	relative error a posteriori metric

Table 1

- [1] *Monte Carlo integration*. https://en.wikipedia.org/wiki/Monte_Carlo_integration.
- [2] A. A. R. ALMOMANI, J. SUN, AND E. BOLLT, *How entropic regression beats the outliers problem in nonlinear system identification*, *Chaos: An Interdisciplinary Journal of Nonlinear Science*, 30 (2020), p. 013107, <https://doi.org/10.1063/1.5133386>.
- [3] S. ANITA AND V. CAPASSO, *Reaction-diffusion systems in epidemiology*, 2017, <https://arxiv.org/abs/1703.02760>.
- [4] L. BONINSEGNA, F. NÜSKE, AND C. CLEMENTI, *Sparse learning of stochastic dynamical equations*, *The Journal of Chemical Physics*, 148 (2018), p. 241723, <https://doi.org/10.1063/1.5018409>, <https://doi.org/10.1063/1.5018409>, <https://arxiv.org/abs/https://doi.org/10.1063/1.5018409>.
- [5] S. L. BRUNTON, J. L. PROCTOR, AND J. N. KUTZ, *Discovering governing equations from data by sparse identification of nonlinear dynamical systems*, *Proceedings of the National Academy of Sciences*, 113 (2016), pp. 3932–3937, <https://doi.org/10.1073/pnas.1517384113>, <http://www.pnas.org/content/113/15/3932>, <https://arxiv.org/abs/http://www.pnas.org/content/113/15/3932.full.pdf>.

- [6] H. CLEVERS, B. ALARCON, T. WILEMAN, AND C. TERHORST, *The t cell receptor/cd3 complex: A dynamic protein ensemble*, Annual Review of Immunology, 6 (1988), pp. 629–662, <https://doi.org/10.1146/annurev.iy.06.040188.003213>, <https://doi.org/10.1146/annurev.iy.06.040188.003213>, <https://arxiv.org/abs/https://doi.org/10.1146/annurev.iy.06.040188.003213>. PMID: 3289580.
- [7] M. DAM, M. BRØNS, J. JUUL RASMUSSEN, V. NAULIN, AND J. S. HESTHAVEN, *Sparse identification of a predator-prey system from simulation data of a convection model*, Physics of Plasmas, 24 (2017), p. 022310, <https://doi.org/10.1063/1.4977057>, <https://doi.org/10.1063/1.4977057>, <https://arxiv.org/abs/https://doi.org/10.1063/1.4977057>.
- [8] D. L. DONOHO, *Compressed sensing*, IEEE Transactions on Information Theory, 52 (2006), pp. 1289–1306, <https://doi.org/10.1109/TIT.2006.871582>.
- [9] M. ELAD, *Sparse and Redundant Representations: From Theory to Applications in Signal and Image Processing*, Springer Publishing Company, Incorporated, 1st ed., 2010.
- [10] L. C. EVANS, *Partial differential equations*, American Mathematical Society, Providence, R.I., 2010.
- [11] K. FRISTON, L. HARRISON, AND W. PENNY, *Dynamic causal modelling*, NeuroImage, 19 (2003), pp. 1273–1302, [https://doi.org/https://doi.org/10.1016/S1053-8119\(03\)00202-7](https://doi.org/https://doi.org/10.1016/S1053-8119(03)00202-7), <http://www.sciencedirect.com/science/article/pii/S1053811903002027>.
- [12] C. GARDINER, *Stochastic Methods*, Springer-Verlag Berlin Heidelberg, 2009.
- [13] T. HASHIMOTO, D. GIFFORD, AND T. JAAKKOLA, *Learning population-level diffusions with generative recurrent networks*, in Proceedings of the 33 rd International Conference on Machine Learning, New York, NY, USA, 2016. JMLR: W CP volume 48, 2016.
- [14] M. HOFFMANN, C. FRÖHNER, AND F. NOÉ, *Reactive syndy: Discovering governing reactions from concentration data*, bioRxiv, (2018), <https://doi.org/10.1101/442095>, <https://www.biorxiv.org/content/early/2018/10/13/442095>, <https://arxiv.org/abs/https://www.biorxiv.org/content/early/2018/10/13/442095.full.pdf>.
- [15] R. JORDAN, D. KINDERLEHRER, AND F. OTTO, *The variational formulation of the fokker–planck equation*, SIAM Journal on Mathematical Analysis, 29 (1998), pp. 1–17, <https://doi.org/10.1137/S0036141096303359>, <https://doi.org/10.1137/S0036141096303359>, <https://arxiv.org/abs/https://doi.org/10.1137/S0036141096303359>.
- [16] A. KLIMOVSKAIA, S. GANSCHA, AND M. CLAASSEN, *Sparse regression based structure learning of stochastic reaction networks from single cell snapshot time series*, PLOS Computational Biology, 12 (2016), pp. 1–20, <https://doi.org/10.1371/journal.pcbi.1005234>, <https://doi.org/10.1371/journal.pcbi.1005234>.
- [17] S. KRISHNASWAMY, M. H. SPITZER, M. MINGUENEAU, S. C. BENDALL, O. LITVIN, E. STONE, D. PE’ER, AND G. P. NOLAN, *Conditional density-based analysis of t cell signaling in single-cell data*, Science, 346 (2014), <https://doi.org/10.1126/science.1250689>, <https://science.sciencemag.org/content/346/6213/1250689>, <https://arxiv.org/abs/https://science.sciencemag.org/content/346/6213/1250689.full.pdf>.
- [18] P. MA, C. I. CASTILLO-DAVIS, W. ZHONG, AND J. S. LIU, *A data-driven clustering method for time course gene expression data*, Nucleic Acids Research, 34 (2006), pp. 1261–1269, <https://doi.org/10.1093/nar/gkl013>, <https://doi.org/10.1093/nar/gkl013>, <https://arxiv.org/abs/https://academic.oup.com/nar/article-pdf/34/4/1261/4158271/gkl013.pdf>.
- [19] S. MA, S. LIU, H. ZHA, AND H. ZHOU, *Learning stochastic behaviour of aggregate data*, 2020, <https://arxiv.org/abs/2002.03513>.
- [20] N. M. MANGAN, T. ASKHAM, S. L. BRUNTON, J. N. KUTZ, AND J. L. PROCTOR, *Model selection for hybrid dynamical systems via sparse regression*, Proc. R. Soc. A, (2019), <https://doi.org/10.1098/rspa.2018.0534>, <https://doi.org/10.1098/rspa.2018.0534>.
- [21] E. MARCO, R. L. KARP, G. GUO, P. ROBSON, A. H. HART, L. TRIPPA, AND G.-C. YUAN, *Bifurcation analysis of single-cell gene expression data reveals epigenetic landscape*, Proceedings of the National Academy of Sciences, (2014), <https://doi.org/10.1073/pnas.1408993111>, <https://www.pnas.org/content/early/2014/12/10/1408993111>, <https://arxiv.org/abs/https://www.pnas.org/content/early/2014/12/10/1408993111.full.pdf>.
- [22] Y. PANTAZIS AND I. TSAMARDINOS, *A unified approach for sparse dynamical system inference from temporal measurements*, Bioinformatics, 35 (2018), pp. 3387–3396, <https://doi.org/10.1093/bioinformatics/btz065>, <https://doi.org/10.1093/bioinformatics/btz065>, <https://arxiv.org/abs/http://oup.prod.sis>.

- lan/bioinformatics/article-pdf/35/18/3387/30024451/btz065.pdf.
- [23] J. RAMSAY AND G. HOOKER, *Dynamic Data Analysis*, Springer-Verlag New York, 2017, <https://doi.org/10.1007/978-1-4939-7190-9>.
- [24] J. O. RAMSAY, G. HOOKER, D. CAMPBELL, AND J. CAO, *Parameter estimation for differential equations: a generalized smoothing approach*, *Journal of the Royal Statistical Society: Series B (Statistical Methodology)*, 69 (2007), pp. 741–796, <https://doi.org/10.1111/j.1467-9868.2007.00610.x>, <https://rss.onlinelibrary.wiley.com/doi/abs/10.1111/j.1467-9868.2007.00610.x>, <https://arxiv.org/abs/https://rss.onlinelibrary.wiley.com/doi/pdf/10.1111/j.1467-9868.2007.00610.x>.
- [25] S. H. RUDY, S. L. BRUNTON, J. L. PROCTOR, AND J. N. KUTZ, *Data-driven discovery of partial differential equations*, *Science Advances*, 3 (2017), <https://doi.org/10.1126/sciadv.1602614>, <http://advances.sciencemag.org/content/3/4/e1602614>, <https://arxiv.org/abs/http://advances.sciencemag.org/content/3/4/e1602614.full.pdf>.
- [26] H. SCHAEFFER, *Learning partial differential equations via data discovery and sparse optimization*, *Proceedings. Mathematical, physical, and engineering sciences*, 473 (2017), p. 20160446, <https://doi.org/10.1098/rspa.2016.0446>, <http://europemc.org/articles/PMC5312119>.
- [27] H. SCHAEFFER, R. CAFLISCH, C. D. HAUCK, AND S. OSHER, *Sparse dynamics for partial differential equations*, *Proceedings of the National Academy of Sciences*, 110 (2013), pp. 6634–6639, <https://doi.org/10.1073/pnas.1302752110>, <http://www.pnas.org/content/110/17/6634>, <https://arxiv.org/abs/http://www.pnas.org/content/110/17/6634.full.pdf>.
- [28] H. SCHAEFFER AND S. G. MCCALLA, *Sparse model selection via integral terms*, *Phys. Rev. E*, 96 (2017), p. 023302, <https://doi.org/10.1103/PhysRevE.96.023302>, <https://link.aps.org/doi/10.1103/PhysRevE.96.023302>.
- [29] J. SUN, D. TAYLOR, AND E. M. BOLLT, *Causal network inference by optimal causation entropy*, *SIAM Journal on Applied Dynamical Systems*, 14 (2015), pp. 73–106, <https://doi.org/10.1137/140956166>, <https://doi.org/10.1137/140956166>.
- [30] J. P. TAYLOR-KING, A. N. RISETH, W. MACNAIR, AND M. CLAASSEN, *Dynamic distribution decomposition for single-cell snapshot time series identifies subpopulations and trajectories during ipsc reprogramming*, *PLOS Computational Biology*, 16 (2020), pp. 1–21, <https://doi.org/10.1371/journal.pcbi.1007491>, <https://doi.org/10.1371/journal.pcbi.1007491>.
- [31] V. TERESHKO, *Reaction-diffusion model of a honeybee colony’s foraging behaviour*, in *Parallel Problem Solving from Nature PPSN VI*, M. Schoenauer, K. Deb, G. Rudolph, X. Yao, E. Lutton, J. J. Merelo, and H.-P. Schwefel, eds., Berlin, Heidelberg, 2000, Springer Berlin Heidelberg, pp. 807–816.
- [32] R. TIBSHIRANI, *Regression shrinkage and selection via the lasso*, *Journal of the Royal Statistical Society. Series B (Methodological)*, 58 (1996), pp. 267–288, <http://www.jstor.org/stable/2346178>.
- [33] J. A. TROPP AND A. C. GILBERT, *Signal recovery from random measurements via orthogonal matching pursuit*, *IEEE Transactions on Information Theory*, 53 (2007), pp. 4655–4666.
- [34] C. WEINREB, S. WOLOCK, B. K. TUSI, M. SOCOLOVSKY, AND A. M. KLEIN, *Fundamental limits on dynamic inference from single-cell snapshots*, *Proceedings of the National Academy of Sciences*, 115 (2018), pp. E2467–E2476, <https://doi.org/10.1073/pnas.1714723115>, <https://www.pnas.org/content/115/10/E2467>, <https://arxiv.org/abs/https://www.pnas.org/content/115/10/E2467.full.pdf>.